IOP Publishing New J. Phys. 26 (2024) 033017 https://doi.org/10.1088/1367-2630/ad2fff

New Journal of Physics
The open access journal at the forefront of physics

Deutsche Physikalische Gesellschaft DPG
IOP Institute of Physics

Published in partnership with: Deutsche Physikalische Gesellschaft and the Institute of Physics

OPEN ACCESS

RECEIVED
7 December 2023

REVISED
26 February 2024

ACCEPTED FOR PUBLICATION
4 March 2024

PUBLISHED
15 March 2024

PAPER

Experimental determination of the hafnium L-subshell fundamental parameters using the holistic approach

Nils Wauschkuhn[1], **Heiko Gundlach**[2] **and Philipp Hönicke**[1,3,*]

[1] Physikalisch-Technische Bundesanstalt (PTB), Abbestr. 2-12, 10587 Berlin, Germany
[2] Technische Universität Berlin, Hardenbergstraße 36a, 10623 Berlin, Germany
[3] Helmholtz-Zentrum Berlin (HZB), Hahn-Meitner-Platz 1, 14109 Berlin, Germany
[*] Author to whom any correspondence should be addressed.

E-mail: philipp.hoenicke@ptb.de

Keywords: hafnium, fluorescence yield, Coster–Kronig, Auger yield, fundamental parameter, subshell-photoionization cross section, subshell fluorescence production yield

Abstract

By employing the recently demonstrated new holistic approach, the atomic fundamental parameters (FPs) of the three Hf-L subshells were experimentally determined using the radiometrically calibrated instrumentation of the Physikalisch-Technische Bundesanstalt. The Coster–Kronig factors, the L-subshell fluorescence yields, the L-subshell Auger yields, the subshell-photoionization cross sections, and the subshell fluorescence production cross sections were determined by means of photon energy dependent x-ray fluorescence and transmission measurements. The recently demonstrated new holistic evaluation approach allows to determine the FPs with significantly lower uncertainties as compared to the former data evaluation scheme, where only a limited regime of incident photon energies is being probed and the data evaluation scheme is performed in a sequential manner.

1. Introduction

The x-ray atomic fundamental parameters (FPs) such as the fluorescence yields, the photoionization cross section, and other FPs are of high relevance for most quantitative analysis involving the x-ray fluorescence process (XRF). Unfortunately, in most of the available FP databases, the experimentally derived FP values for the different chemical elements are often relatively old, which often means that by employing both state-of-the-art instruments and methods, more reliable data can be obtained. And for some elements, only interpolated from adjacent elements or only theoretically calculated data without an experimental verification is available. Furthermore, the uncertainties of most of these tabulated FP data are either not available or only estimated which directly affects any quantification based on these FPs. To improve this situation, the International initiative on x-ray FPs [1] and others are working on updating and revisiting existing FP databases with new experimentally derived data including reliable uncertainty budgets and state-of-the-art calculations for a number of years now. At the Physikalisch-Technische Bundesanstalt (PTB), well-characterized physically calibrated XRF instrumentation is employed for dedicated FP experiments in order to update existing FP data. Recently, a new holistic data evaluation approach for accessing the FPs for the L-subshells has been demonstrated [2].

This new approach uses a much larger set of experimentally probed photon energies for sample transmission and fluorescence emission as compared to earlier works such as [3]. In addition, it employs a combined data evaluation approach incorporating modern mathematical methods to derive the FPs of interest with drastically reduced experimental uncertainties. This makes quantification applications more accurate and also enables meaningful access to derived FPs such as subshell production cross sections or Auger yields.

In this work, we have applied the new holistic approach to experimentally determine the L-subshell FPs of hafnium, which is an important element for state-of-the-art semiconductor applications [4–6] and other relevant fields [7–9]. The atomic FP data determined in this work can also be found on Zenodo [10].

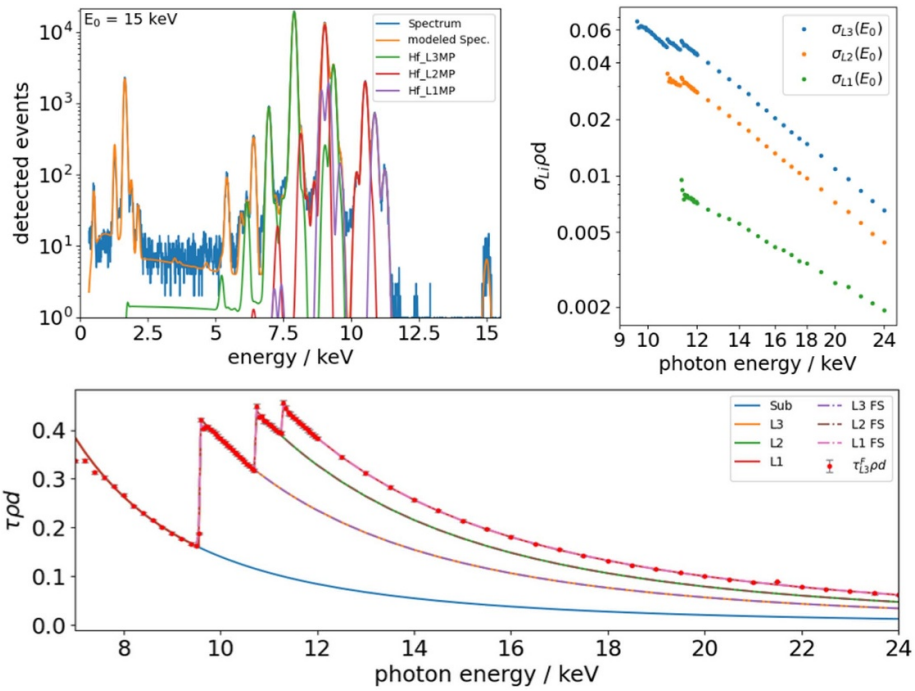

Figure 1. Exemplary fluorescence spectrum for an excitation photon energy of 15 keV as well as the relevant deconvolution components are shown in the upper left panel. The thereby derived sample specific L-subshell fluorescence production cross sections as a function of the excitation energy are shown in the upper right. In the bottom panel, the determined sample specific total photoionization cross section as well as its separation into each component are shown.

2. Holistic experimental approach

For the determination of the L-subshell FPs of hafnium, we have obtained thin film depositions of hafnium oxide on silicon nitride membranes. The silicon nitride windows were obtained from Norcada and have a nominal membrane thickness of 1000 nm. The deposition of HfO_2 was realized by means of electron-beam physical vapor deposition employing a Leybold Optics SYRUSpro710 instrument. The deposition was split into several subsequent runs in order to avoid excessive sample heating and thus a possible failure of the silicon nitride membrane.

Combined transmission and fluorescence experiments were carried out at the BAMline (the beamline of the Bundesanstalt für Materialforschung und -prüfung) [11] of BESSY II (2nd electron storage ring of Berliner Elektronenspeicherring-Gesellschaft für Synchrotronstrahlung) employing the radiometrically calibrated instrumentation of the Physikalisch-Technische Bundesanstalt [12]. The combined transmission and fluorescence experiments were performed using a vacuum chamber equipped with a calibrated silicon drift detector (SDD, with experimentally determined response functions [13] and calibrated detection efficiencies), placed behind a calibrated aperture defining the solid angle of detection. A calibrated photodiode is used to determine the incident photon flux at each employed incident photon energy. The hafnium oxide coated foil as well as a blank reference foil were placed in the center of the vacuum chamber with an angle of 45° with respect to both the incident beam and the SDD.

The photon energy range in transmission measurements spans from below the L_3-shell (in order to obtain the sample's attenuation for the Hf-L fluorescence lines) up to 24 keV, as depicted in figure 1. The photon energy domain for fluorescence measurements also extends from the L_3-shell up to 24 keV. From the photon energy dependent transmission of each foil, sample specific mass attenuation factors $\mu_S(E_0)\rho d$ [14] can be derived and used for the calculation of the attenuation correction factor $M_{i,E0}$ which is then independent from any database values for mass attenuation coefficients. The fluorescence photon flux $\Phi_i^d(E_0)$ is evaluated from the measured fluorescence spectra using a spectral deconvolution procedure based on the experimentally determined detector response functions. They are used to model the relevant fluorescence lines and the relevant background contributions, e.g. bremsstrahlung, originating from photo-electrons. An exemplary fluorescence spectrum for an excitation photon energy of 15 keV as well as the relevant deconvolution components are shown in the upper left panel of figure 1. The various fluorescence lines from each of the three Hf-L subshells are being combined into a fixed line set for a more reliable spectral deconvolution [3].

The deconvolved counts for each line set are normalized to integration time and detection efficiencies in order to determine the detected subshell fluorescence intensities Φ_{Li}^{d} for each subshell. Together with the solid angle of detection $\frac{\Omega}{4\pi}$ and the incident photon flux Φ_0 and the attenuation correction factor M_{Li,E_0}, this allows to derive the sample specific L-subshell fluorescence production cross sections as a function of the excitation energy which are shown in the upper right panel of figure 1

$$\sigma_{L_i}(E_0)\,\rho d = \omega_{L_i}\tau_{L_i}^{\mathrm{eff}}(E_0)\,\rho d = \frac{\Phi_{Li}^{d}(E_0)\,M_{Li,E_0}}{\Phi_0(E_0)\,\frac{\Omega}{4\pi}}. \tag{1}$$

Here, $\tau_{L_i}^{\mathrm{eff}}(E_0)$ is the sample specific effective photoionization cross section, which includes the Coster–Kronig factors depending on the photon energy and ω_{L_i} is the respective fluorescence yield. The attenuation correction factor M_{Li,E_0} is calculated by

$$M_{Li,E_0} = \frac{\left(\frac{\mu_S(E_0)\rho d}{\sin\theta_{in}} + \frac{\mu_S(E_i)\rho d}{\sin\theta_{out}}\right)}{\left(1-\exp\left[-\left(\frac{\mu_S(E_0)\rho d}{\sin\theta_{in}} + \frac{\mu_S(E_i)\rho d}{\sin\theta_{out}}\right)\right]\right)}, \tag{2}$$

where the incident θ_{in} and detection angles θ_{out} as well as the sample specific attenuation coefficients $\mu_S\rho d$ are used. The latter is directly derived from the transmission data.

The effective photoionization cross sections are calculated using each subshell's photoionization cross section and the Coster–Kronig factors as follows:

$$\tau_{L_3}^{\mathrm{eff}}(E_0) = \tau_{L_3}(E_0) + f_{23}\tau_{L_2}(E_0) + [f_{13} + f_{12}f_{23}]\,\tau_{L_1}(E_0) \tag{3}$$

$$\tau_{L_2}^{\mathrm{eff}}(E_0) = \tau_{L_2}(E_0) + f_{12}\tau_{L_1}(E_0) \tag{4}$$

$$\tau_{L_1}^{\mathrm{eff}}(E_0) = \tau_{L_1}(E_0). \tag{5}$$

By using the experimental sample transmission to derive the sample specific mass attenuation coefficients and the following one can determine the sample specific subshell photoionization cross sections by removing the scattering fraction:

$$\tau_{\mathrm{Tot}}(E_0)\,\rho d = \mu_S(E_0)\,\rho d\left[1 - \frac{\sigma_{C,Hf}(E_0) + \sigma_{I,Ru}(E_0)}{\mu_{Hf}(E_0)}\right]. \tag{6}$$

The separation of $\tau_{\mathrm{Tot}}(E_0)\rho d$ into the three L-subshell contributions as well as the lower bound shell's contributions is realized by scaling Ebel polynomials [15] into the transmission dataset as shown in figure 1. These polynomials are exponential functions as shown in equation (7)

$$\tau_{i,E_0} = \exp\left[A_0 + \ln(E_0)A_1 + \ln(E_0)^2A_2 + \ln(E_0)^3A_3 + \ln(E_0)^4A_4 + \ln(E_0)^5A_5\right]. \tag{7}$$

Here, the A_i are the modifieable parameters for scaling the respective subshell's contribution into the experimental $\tau_{\mathrm{Tot}}(E_0)\rho d$ dataset.

To further reduce the number of parameters, one can use the fact that the L_3- and L_2-subshells have very similar energy dependence. Thus, the L_2 contribution can be replaced by a scaled version of L_3. The lower bound shells can be summed up using the coefficients from Ebel *et al* [15] and then modified by multiplying an Ebel polynomial with only the first two or three parameters to allow for slight energy dependence modifications.

For this holistic optimization, one can employ that the derived subshell fluorescence yields must be constant no matter at which photon energy they are calculated and that the subshell ionization cross sections derived from the separation of the transmission data and the ones that can be calculated from the fluorescence data must be the same. Based on these relations, a Markov-Chain-Monte-Carlo (MCMC) [16] algorithm can be employed to find the optimal parameter set consisting of the CK factors as well as the A_i parameters for the subshell photoionization contributions. For further details see [2].

In this work, the three Coster–Kronig factors (according to equations (3)–(5)), a set of 3 parameters for scaling the lower bound shell contributions, and between one and six parameters for the Ebel polynomials of the L_3- and L_1 subshell photoionization cross section are being optimized. One additional free parameter is used to rescale the L_3-subshell photoionization cross section to be used as the L_2-subshell data. This totals to at least 9 and up to 19 free parameters. Depending on the configuration of the free parameter set, the parameters which are not included in the modeling are set to the respective value from the Ebel data for the Hf L-subshells [15].

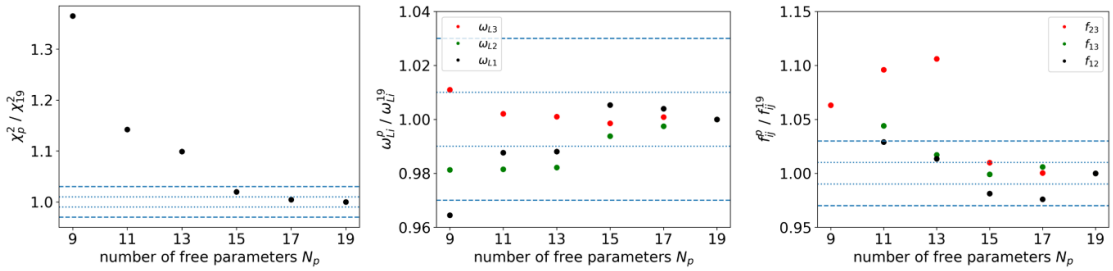

Figure 2. Evolution of different output parameters as a function of the number of free model parameters. The overall χ^2 is shown on the left, the derived subshell fluorescence yields in the middle and the Coster–Kronig factors on the right. Each data point is normalized with respect to the respective results employing the full free parameter set. The three Coster–Kronig factors, a set of 3 parameters for scaling the lower bound shell, the L_2 scaling factor, and the A_0 parameters of the L_3- and L_1-subshell are the minimal parameter set. The dashed and dotted lines depict a $\pm 3\%$ and $\pm 1\%$ level respectively.

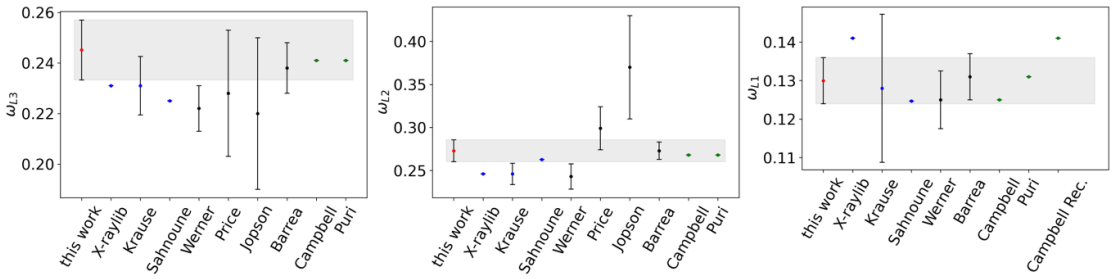

Figure 3. Experimentally determined Hf-L subshell fluorescence yields of this work compared to various values available from compilations (blue) such as X-raylib [17], the Krause database [18] or the work of Sahnoune *et al* [19], from various older experimental determinations (black) [20–23] or from theoretical calculations (green) [24–26]. The grey shaded area depicts the uncertainty regime of our results.

3. Results and discussion

As a first step in the holistic data evaluation scheme, the convergence of the results as a function of the number of free parameters N_p is studied. This is necessary, as too few free parameters will not allow to reconstruct the correct photon energy dependence of the subshell photoionization cross sections, which will introduce artifacts into the derived FPs. On the other hand, too many free parameters may allow to reconstruct erroneous transmission data due to effects such as stray light or other instabilities to be interpreted as a changed photon energy dependence of the subshell photoionization cross sections. This may also lead to wrongly derived FP data.

Both of these potential artifacts can be assessed by studying the performance of the data evaluation for the different sets of parameters as shown in figure 2. The overall χ^2 normalized to the value obtained for $N_p = 19$ is shown on the left and it nicely converges for higher values of N_p. A similar behavior can be observed for the three CK values on the right. The fluorescence yield values, which are shown in the middle, show only a very minor dependence on the N_p value.

For the following FP results, the $N_p = 15$ are picked as they are of similar reliability as compared to the results obtained at $N_p = 19$ but an influence due to a potential over interpretation of the experimental photon energy dependence in the sample transmission is less likely.

3.1. Determination of fluorescence yields

The fluorescence yields for the three L-subshells are being calculated at each incident photon energy according to equation (1). The final result is then derived by averaging over the full energy range. The results obtained in this work are shown in figure 3 in comparison to common literature data. The grey shaded area depicts the uncertainty regime of our results.

The experimentally determined Hf-L subshell fluorescence yields deviate to some extent from the data compiled in X-raylib [17] which is usually the most reliable and most up-to-date compilation. In the case of Hf, both the L_3 and L_2 shell values are larger as compared to X-raylib whereas the L_1 shell result is lower. With respect to the Krause data, the agreement at least with respect to the stated uncertainty budgets is better especially for L_1. In the case of Hf, the theoretically derived data is in very good agreement with our results for all three L-subshells. Also for the fluorescence yields determined by Barrea *et al* [23] a good agreement for

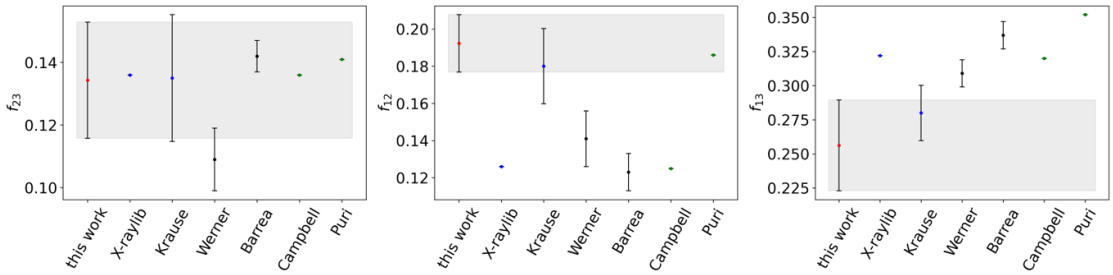

Figure 4. Comparison of the Coster–Kronig factors of this work with the corresponding values from literature compilations [17, 18], experiments [20, 23] and theoretical calculations [24–26]. The grey shaded area depicts the uncertainty regime of our results.

Table 1. Overview of the achieved relative uncertainties for the Hf-L CK factors in this work compared to the estimates by Krause [18] for the tabulated CK factors.

Parameter	rel. uncertainty estimate Krause	rel. uncertainty this work
f_{23}	15%	14%
f_{12}	20%	8%
f_{13}	10%	13%

all three shells is found. The other available experimental data show reasonable agreement for L_3 considering the stated uncertainties, less good agreement for L_2, and good agreement for the L_1 data.

3.2. Determination of Coster–Kronig factors

The Coster–Kronig factors determined in this work are compared to values from the literature in figure 4. Here, a good agreement to the X-raylib value as well as the theoretical calculations is observed for f_{23}. The experimentally determined value of Barrea *et al* also agrees very well with our result. For f_{12} and f_{13}, more deviations between the present result and the different literature sources can be observed. A significant deviation with respect to X-raylib is found whereas the Krause data agrees within the uncertainties with our results. All other available results do not agree within our stated uncertainty except for the theoretical calculation of Puri for f_{12}. Considering the experimental results of Werner *et al* and Barrea *et al* it seems as if their stated uncertainty budgets may not contain all relevant contributions or that systematic errors are still present. Their works are based on a data evaluation strategy were only the region around the three L-shells is being probed. As already stated in our earlier work on the Ru-L shell parameters [2], this approach is very sensitive to extrapolation errors of the subshell photoionization cross sections. Depending on how they were determined in these works, this may explain the observed deviations. With the present holistic approach the accuracy of these extrapolations is probed during the optimization and a much wider photon energy range is probed. This should thus be more reliable as compared to how it was usually done.

But more importantly, the experimental uncertainties of our new results are drastically reduced compared to what would have been provided employing the classical approach for FP determination. Typically, the achievable uncertainties for the CK factors were at best in the order of the Krause estimates [18] and usually much larger [3, 27, 28]. With the holistic approach the achieveable uncertainties for the CK factors can be significantly reduced [2] as compared to the conventional data evaluation approach. For the Hf-L subshells, they are now in the 10% regime as shown in table 1, which is comparable to the Krause estimates or even lower in the case of f_{12}.

3.3. Determination of Auger yields

Employing the relation

$$\omega_{Li} + f_{Lij} + a_{Li} = 1 \tag{8}$$

the Auger yield a_{Li} as the probability for an Auger decay following an ionization of the L_i-shell can be derived by subtracting the determined fluorescence yield and relevant Coster–Kronig factors from unity. As the uncertainties of the experimental fluorescence yields and the CK factors add up for a combined uncertainty of the Auger yields, such a calculation only provides a meaningful result if both uncertainty contributions are reasonably small. As already mentioned, this was not the case employing the classical FP determination approach. With the new holistic approach [2], this can be realized and the resulting Auger yields for the Hf L-shells can be derived. The resulting Auger yields for the Hf-L shells are shown in figure 5.

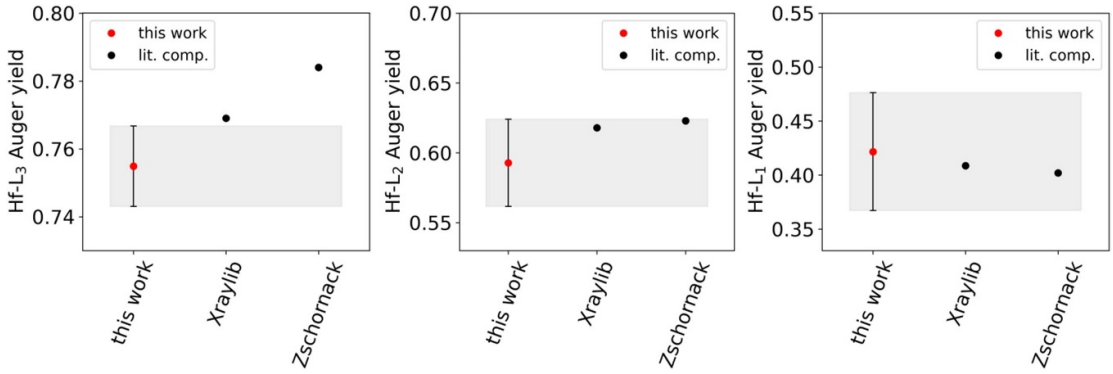

Figure 5. Comparison of the Hf-L subshell Auger yields determined in this work with values from X-raylib [17] and the handbook of x-ray data [29]. The grey shaded area depicts the uncertainty regime of our results.

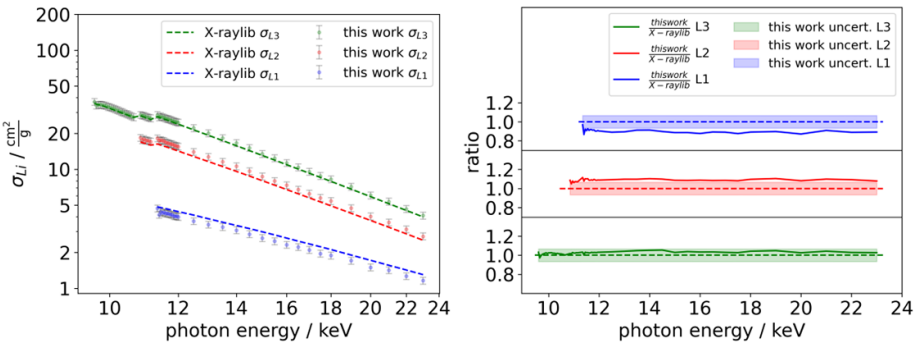

Figure 6. Comparison of the Hf-L subshell fluorescence production yields experimentally determined in this work with data from X-raylib [17]. The left panel shows a direct comparison whereas the right one depicts ratios between our data and X-raylib. The green-, red- and blue shaded areas depict the uncertainty regimes of our data.

The tabulated Hf-L_3 Auger yields are slightly larger than our result. The value from X-raylib is in better agreement with our result as the value from Zschornack [29]. For the other two subshells, our results agree well with the two tabulated datasets within our stated uncertainty regime (grey shaded areas).

3.4. Determination of subshell fluorescence production yields

Of course, one can also use the normalized term from equation (1) and similar terms for the L_2- and L_1-subshells to have a direct look at the fluorescence production cross sections for each subshell and each studied incident photon energy. Here, the areal mass of Hf present on the sample has been quantified and removed from the sample specific subshell fluorescence production cross sections. The resulting data is shown in figure 6 in comparison to tabulated fluorescence production cross sections from X-raylib [17].

The subshell fluorescence production cross sections for the L_3-subshell agree reasonably well within the uncertainty regime of our data (green-, red- and blue shaded areas in the ratio plots) throughout the full studied photon energy range. Also at the L_2 and L_1 absorption edges, where the Coster–Kronig contributions start to appear, a good agreement is found. For the L_2 and L_1 data, the agreement is less good. Both X-raylib datasets lie slightly outside of our uncertainty regimes with the X-raylib L_2 data being lower and the L_1 data being higher than our production cross sections.

3.5. Determination of subshell-photoionization cross sections

Of course one can also solve equation (1) and its L_2- and L_1-subshell counterparts for $\tau_{L_i}^{\mathrm{eff}}(E_0)\rho d$, decouple the Coster–Kronig contributions and remove the samples areal mass to isolate the subshell photoionization cross sections for the three Hf-L subshells. The results are plotted in figure 7 in comparison to different typical literature sources.

Here, very similar observations as compared to the production cross sections can be seen. The L_3-subshell cross section agrees very well with the calculations by Scofield [30], which is the basis for common databases such as X-raylib. For the L_2-subshell, our data is slightly lower than Scofield but they still agree considering our uncertainty budget. Regarding fixed jump ratio based datasets such as the Elam tables [31], the expected deviations are also observed here. But this is not surprising as the energetic decay for the

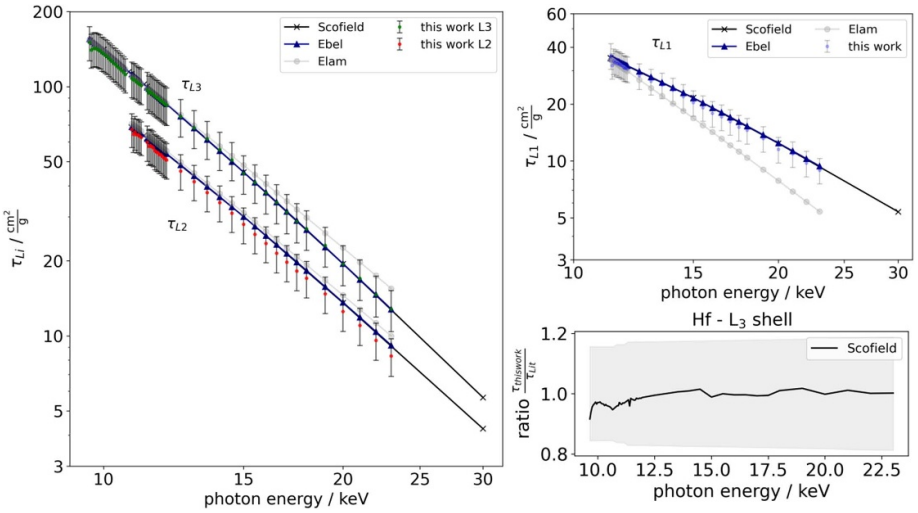

Figure 7. Comparison of the experimentally determined Hf-L subshell photoionization cross sections with different common literature datasets such as the theoretical calculations by [30], which are the basis for the Ebel data [15] and X-raylib. The Elam data [31] is a representative of the fixed jump ratio based datasets which do not describe the energetic behavior correctly. Bottom right: ratio of the L_3 subshell-photoionization cross section of this work and the Scofield data.

three L-subshell photoionization cross sections is not the same. This is even more obvious for the L_1-shell, which is shown in the upper right panel of figure 7. Here, the jump ratio based cross sections are totally off, especially for higher photon energies. The Scofield and Ebel [15] data, which are based on one another, describe our experimental data very well. Similar findings were observed also for other elements [2, 32, 33].

4. Conclusions

In the present work, the recently demonstrated novel approach for the experimental determination of x-ray FPs [2] was used to experimentally determine relevant atomic FPs for the three Hf-L subshells. Each subshell's fluorescence yield, the three Coster–Kronig factors, the Auger yields as well as the subshell fluorescence production cross sections and the subshell photoionization cross sections have been determined and compared to available data in the literature.

The approach is based on transmission and fluorescence measurements over much wider range of incident photon energies as compared to the conventional approach. Here, the photon energy range extents far above the absorption shells of interest, whereas in the conventional approach only a few hundred eV above the L_1 threshold is usually being used. In addition, the data evaluation approach is different here as compared to earlier works. Both datasets are evaluated by a unified parameter optimization rather than in a sequential approach as it used to be done in conventional FP determinations. This helps to ensure a more reliable extrapolation of the various subshell photoionization cross sections. In addition, the experimental uncertainties are evaluated employing Markov-Chain-Monte-Carlo based analysis.

These developments allow for a significant reduction of the overall achievable uncertainties, especially for the Coster–Kronig factors. The reduced uncertainties consequently allow for a meaningful determination of nearly all relevant x-ray FPs of the Hf-L subshells. In the case of the Hf-L subshells, not only the subshell fluorescence yields and Coster–Kronig factors could be determined but also the subshell Auger yields as well as subshell fluorescence production—and subshell photoionization cross sections. All of the determined FP data in this work can be found on Zenodo [10] for download.

Data availability statement

The data cannot be made publicly available upon publication because they are not available in a format that is sufficiently accessible or reusable by other researchers. The data that support the findings of this study are available upon reasonable request from the authors. The atomic FP data determined in this work can be found on Zenodo [10].

Acknowledgment

This project has received funding from the ECSEL Joint Undertaking (JU) IT2 under Grant Agreement No 875999. The JU receives support from the European Union's Horizon 2020 research and innovation program and the Netherlands, Belgium, Germany, France, Austria, Hungary, the United Kingdom, Romania and Israel. In addition, this project has received funding from the European Union's Horizon 2020 research and innovation programme under Grant Agreement No 861857 CHALLENGES as well as from the Horizon Europe under Grant Agreement 101096772-14ACMOS.

ORCID iDs

Nils Wauschkuhn https://orcid.org/0000-0001-6187-3786
Philipp Hönicke https://orcid.org/0000-0002-0712-903X

References

[1] 2021 International initiative on x-ray fundamental parameters (available at: www.exsa.hu/fpi.php) (Accessed 03 June 2022)
[2] Hönicke P 2023 A novel and holistic approach for experimental x-ray fundamental parameter determination—the ru L-shell *New J. Phys.* **25** 073012
[3] Kolbe M, Hönicke P, Müller M and Beckhoff B 2012 L-subshell fluorescence yields and Coster–Kronig transition probabilities with a reliable uncertainty budget for selected high- and medium-z elements *Phys. Rev.* A **86** 042512
[4] Choi J H, Mao Y and Chang J P 2011 Development of hafnium based high-k materials—a review *Mater. Sci. Eng. R* **72** 97–136
[5] Böscke T S, Müller J, Bräuhaus D, Schröder U and Böttger U 2011 Ferroelectricity in hafnium oxide thin films *Appl. Phys. Lett.* **99** 102903
[6] Singh S, Raj Solay L, Anand S, Kumar N, Ranjan R and Singh A 2023 Implementation of gate-all-around gate-engineered charge plasma nanowire fet-based common source amplifier *Micromachines* **14** 1357
[7] Maggiorella L, Barouch G, Devaux C, Pottier A'es, Deutsch E, Bourhis J, Borghi E and Levy L 2012 Nanoscale radiotherapy with hafnium oxide nanoparticles *Future Oncol.* **8** 1167–81
[8] Dutta S, Buragohain P, Glinsek S, Richter C, Aramberri H, Haidong L, Schroeder U, Defay E, Gruverman A and Íñiguez J 2021 Piezoelectricity in hafnia *Nat. Commun.* (https://doi.org/10.1038/s41467-021-27480-5)
[9] Shikov A, Bocharov O, Arzhakova V, Bezumov V, Perlovich Y and Isaenkova M 2003 Use of hafnium in control elements of nuclear reactors and power units *Metal Sci. Heat Treat.* **45** 300–3
[10] Hönicke P, Wauschkuhn N and Gundlach H 2023 Experimental determination of the hafnium l-subshell fundamental parameters using the holistic approach (https://doi.org/10.5281/zenodo.10203887)
[11] Görner W, Hentschel M P, Müller B R, Riesemeier H, Krumrey M, Ulm G, Diete W, Klein U and Frahm R 2001 BAMline: the first hard x-ray beamline at BESSY II *Nucl. Instrum. Methods* A **467–468** 703–6
[12] Beckhoff B 2022 Traceable characterization of nanomaterials by x-ray spectrometry using calibrated instrumentation *Nanomaterials* **12** 2255
[13] Scholze F and Procop M 2001 Measurement of detection efficiency and response functions for an Si(Li) x-ray spectrometer in the range 0.1–5 kev *X-Ray Spectrom.* **30** 69–76
[14] Unterumsberger R, Hönicke P, Colaux J, Jeynes C, Wansleben M, Müller M and Beckhoff B 2018 Accurate experimental determination of gallium k- and L3-shell xrf fundamental parameters *J. Anal. At. Spectrom.* **33** 1003–13
[15] Ebel H, Svagera R, Ebel M F, Shaltout A and Hubbell J H 2003 Numerical description of photoelectric absorption coefficients for fundamental parameter programs *X-Ray Spectrom.* **32** 442–51
[16] Foreman-Mackey D, Hogg D W, Lang D and Goodman J 2013 emcee: the MCMC hammer *Publ. Astron. Soc. Pac.* **125** 306–12
[17] Schoonjans T, Brunetti A, Golosio B, Sanchez del Rio M, Solé V A, Ferrero C and Vincze L 2011 The xraylib library for x-ray-matter interactions. Recent developments *Spectrochim. Acta* B **66** 776–84
[18] Krause M O 1979 Atomic radiative and radiationless yields for k and l shells *J. Phys. Chem. Ref. Data* **8** 307–27
[19] Sahnoune Y, Kahoul A, Kasri Y, Deghfel B, Medjadi D E, Khalfallah F, Daoudi S, Aylikçi V, Küp Aylikçi N and Nekkab M 2016 L1, l2 and l3 subshell fluorescence yields: updated database and new empirical values *Radiat. Phys. Chem.* **125** 227–51
[20] Werner U and Jitschin W 1988 L-vacancy decay in heavy elements ($72 \leqslant z \leqslant 82$) by the synchrotron photoionization method *Phys. Rev.* A **38** 4009–18
[21] Price R E, Mark H and Swift C D 1968 Measurements of L_2- and L_3-subshell fluorescence yields in heavy elements *Phys. Rev.* **176** 3–10
[22] Jopson R C, Khan J M, Mark H, Swift C D and Williamson M A 1964 Fluorescence yields of the L_{II} and L_{III} shells in heavy elements *Phys. Rev.* **133** A381–4
[23] Barrea R A, Perez C A and Sanchez H J 2002 Hafnium L-subshell Coster–Kronig and fluorescence yields determination by synchrotron photoionization *Spectrochim. Acta* B **57** 999–1008
[24] Campbell J L 2003 Fluorescence yields and Coster–Kronig probabilities for the atomic l subshells *Atom. Data Nucl. Data* **85** 291–315
[25] Campbell J L 2009 Fluorescence yields and Coster–Kronig probabilities for the atomic l subshells. Part II: The L1 subshell revisited *Atom. Data Nucl. Data* **95** 115–24
[26] Puri S, Mehta D, Chand B, Singh N and Trehan P N 1993 L shell fluorescence yields and Coster–Kronig transition probabilities for the elements with $25 < z < 96$ *X-Ray Spectrom.* **22** 358–61
[27] Kolbe M and Hönicke P 2015 Fundamental parameters of Zr and ti for a reliable quantitative x-ray fluorescence analysis *X-Ray Spectrom* **44** 217–20
[28] Wauschkuhn N, Frenzel K, Beckhoff B and Hönicke P 2023 Experimental determination of tantalum L-shell fluorescence yields and coster–kronig transition probabilities *J. Anal. At. Spectrom.* **38** 197–203
[29] Zschornack G H (ed) 2007 *Handbook of x-ray Data* (Springer)

[30] Scofield J H 1973 Theoretical photoionisation cross sections from 1 to 1500 kev UCRL-51326 (https://doi.org/10.2172/4545040)
[31] Elam W T, Ravel B D and Sieber J R 2002 A new atomic database for x-ray spectroscopic calculations *Radiat. Phys. Chem.* **63** 121–8
[32] Hönicke P, Kolbe M, Müller M, Mantler M, Krämer M and Beckhoff B 2014 Experimental verification of the individual energy dependencies of the partial L-shell photoionization cross sections of Pd and Mo *Phys. Rev. Lett.* **113** 163001
[33] Hönicke P, Kolbe M and Beckhoff B 2016 What are the correct l-subshell photoionization cross sections for quantitative x-ray spectroscopy? *X-Ray Spectrom.* **45** 207–11